Surface reconstruction stability and configurational disorder on Bi-terminated GaAs(001)

Adam Duzik,[*] John C. Thomas,[†] Anton van der Ven,[‡] and Joanna M. Millunchick[§]

Department of Materials Science and Engineering, The University of Michigan, 2300 Hayward St., HH Dow Bldg., Ann Arbor, Michigan 48109, USA

(Received 16 October 2012; published 28 January 2013)

We developed a rigorous and exhaustive method for calculating the 0 K surface phase diagram of Bi/GaAs(001) by using density functional theory in conjunction with the cluster expansion formalism. In a search for ground-state alloy configurations of low energy surface structure prototypes, we found that the (2×1), $\alpha 2(2 \times 4)$, and $\beta 2(2 \times 4)$ structures possess only a few stable configurations, though each is stable over a wide range of chemical potential. In contrast, the $c(4 \times 4)$ and (4×3) structures exhibit many stable configurations, suggesting their tendency towards configurational disorder at finite temperature. Monte Carlo simulations confirm a continuous disordering of the (4×3) reconstruction with increasing temperature that comes to completion well below typical MBE growth conditions, in contrast to the (2×1) structure, which remains ordered at high temperature. The calculated zero Kelvin phase diagram and finite temperature Monte Carlo results are in excellent agreement with STM in this work and experimental observations seen elsewhere. Furthermore, these results provide important insights into challenges posed by growth of GaAsBi alloys, namely Bi incorporation, $CuPt_B$ ordering, and Bi clustering.

DOI: 10.1103/PhysRevB.87.035313 PACS number(s): 68.35.B−, 31.15.A−, 68.35.Md, 68.37.Ef

I. INTRODUCTION

Bi-containing III-V semiconductor alloys have attracted intense interest within the last decade. Incorporation of Bi significantly reduces the band gap of GaAs by ∼84 meV/%Bi while preserving its high electron mobility.[1,2] The reduced band gap is largely insensitive to temperature, and the large spin-orbit coupling of Bi suppresses Auger recombination and enables possible spintronic devices.[3,4] Such behavior has been attributed to Bi_{Ga} antisite defects,[5,6] but extended x-ray absorption fine spectra (EXAFS)[7] and transmission electron microscopy[8] results suggest that Bi substitutes for As in $GaAs_{1-x}Bi_x$. Bi has been shown to either cluster or order on the bulk GaAs lattice depending on the composition. At Bi compositions of $0.01 < x < 0.025$, Bi atoms preferentially form dimers or tetramers on the Group V sublattice.[7] At $0.03 < x < 0.10$, $GaAs_{1-x}Bi_x$ develops $CuPt_B$ ordering, presumably induced by the (2×1) surface reconstruction, but at $x = 0.13$, the ordering disappears and coarse phase separation occurs.[9]

A number of observations suggest that the atomic structure at the surface significantly influences the bulk structure, interfacial uniformity, and surface morphology. A major difficulty of accurately characterizing the atomic structure of a multicomponent surface lies in the necessity of considering both structure and configuration. This has been successfully overcome in several systems, including the Mn-doped GaAs (110),[10,11] the Co_2MnSi/GaAs(001),[12] the InGaAsN,[13] in Si-doped bulk GaAs,[14] and both undoped and Si-doped GaAs nanowire systems.[15] This was possible due to experimental observations in these systems. In the present Bi/GaAs system, several experimental observations have already been established. Bi possesses a strong tendency to surface segregate without incorporating, acting as a surfactant on GaAs, InGaAs,[16] and GaAsN.[17] Bi has been shown to significantly disrupt the $CuPt_B$ ordering in InGaP[18] and alter the step density and structure to decrease roughness on the micron length scale in GaAs,[19] both of which have been attributed to Bi-induced surface reconstructions. There are a number of surface reconstructions that have been observed on this surface. The (2×1) reconstruction appears when Bi is deposited on a metal-terminated surface and has been studied extensively using scanning tunneling microscopy (STM) and density functional theory (DFT).[20–23] The $(n \times 3)$ reconstruction is observed to occur at higher As overpressures, and Duzik *et al.* recently proposed a structural model of that reconstruction.[19] Despite these advances, a full understanding of Bi-containing surface reconstructions on GaAs and their direct impact on the surface morphology and compositional uniformity in the bulk has yet to be established.

The atomic structure of the Bi/GaAs surface, which is described by the size and shape of the unit cell on the surface and the local bonding topology of surface atoms, is specified by the surface reconstruction prototype. The configuration of a given prototype specifies one of the many ways to arrange the component species at the undercoordinated sites of the prototype. In general, these sites can undergo isovalent substitution of Bi for As or nonisovalent substitution of a Group V species (i.e., As or Bi) for Ga. Understanding the effect of species configuration on reconstruction stability and surface order will yield insights into bulk ordering, phase separation, and clustering, as those phenomena are hypothesized to be related to the details of the surface structure.

This paper presents a rigorous prediction of the thermodynamically stable configurations of Bi-terminated GaAs(001) at 0 K from first principles. Although theoretical techniques such as DFT enable prediction of surface phase stability from first principles, they are too computationally intensive to enable a thorough search of the multitude of plausible configurations of each prototype. To reduce the number of DFT calculations, the cluster expansion method was used to guide the search for ground-state configurations of the surface. A surface phase diagram was constructed from the DFT energies of the configurations predicted by the cluster expansion. Finally, finite temperature effects on configurational surface order are predicted through Monte Carlo simulations, which favorably

compares to experimentally produced STM images of the Bi/GaAs surface reconstruction.

II. DFT SIMULATIONS

The first step in constructing a phase diagram of the surface reconstructions is to assemble a set of candidate prototypes. These are typically determined from experimental observations such as reflective high energy electron diffraction (RHEED), which provides information on the size and shape of the surface unit cell, but not the details of the structure. STM provides valuable insight into the arrangement of atoms in the unit cell, but experimentally discerning details of the species at each atomic site is more difficult. Past work has relied on intuited structures and configurations to form the set of candidate prototypes. Naturally, this is not an exhaustive approach, as many structures and configurations are likely to be overlooked. For instance, Laukkenen *et al.* calculated a Bi/GaAs phase diagram based upon their experimental results at low As overpressure.[20] Thus, they did not take the $(n \times 3)$ prototype into account.

In this work, we employ a fully comprehensive approach to ensure that all possible structures are considered. We begin by enumerating all possible reconstruction prototypes that have the surface unit cell size and shape suggested by experimentally obtained diffraction patterns. The enumerated structures are constrained to have only known structural motifs of anion-terminated III-V surfaces, including surface dimers and backbonds and are prevented from having unphysical motifs such as subsurface vacancies and severely undercoordinated sites.[24]

The resulting database was screened for low energy prototypes using the electron counting model[25] and DFT calculations, assuming anion rich conditions. The $\alpha 2(2 \times 4)$, $\beta 2(2 \times 4)$, and $c(4 \times 4)$ reconstructions, illustrated in Figs. 1(a)–1(c), were identified via this method as the most likely prototypes in their respective unit cells, in agreement with prior work.[26] We also considered the observed Bi-induced reconstructions, namely the (2×1), $\alpha 2(2 \times 4)$,[20–23] (1×3), and (2×3) reconstructions.[16,19,27] The Ga rich $\zeta(4 \times 2)$ reconstruction[28] [Fig. 1(d)] was included as a bound on the anion poor surface but does not conform to the anion rich motifs assumed for the enumeration method.

Enumeration of (2×1) reconstructions [Fig. 1(e)] produced only one possibility that obeys the structural rules. This configuration is metallic, and does not obey the electron counting model owing to a deficit of one electron per unit cell. This is in agreement with scanning tunneling spectroscopy results that confirm the metallic nature of the (2×1) surface.[20] Out of the 893 enumerated prototypes with (2×3) and (4×3) unit cells, only 123 obey the electron counting rule. The lowest energy prototype found is depicted in Fig. 1(f). A (1×3) unit cell was not identified that obeys the structural rules. However, shifting the (4×3) unit cells along the $[\bar{1}10]$ can result in either a (2×3) or (1×3) RHEED pattern,[29] suggesting that a (4×3) reconstruction prototype can be used to explain experimental results.

Within each reconstruction prototype, a Ga, As, or Bi atom can occupy each threefold coordinated surface site without affecting the electron counting rule, allowing many possible configurations for a given composition of the surface. For example, there are over 30 000 symmetrically distinct configurations of the (4×3) prototype depicted in Fig. 1(f), with many low energy configurations of these sites differing by no more than $\sim$20 meV/A(1×1), nearly an order of magnitude smaller than energy variations due to differences in reconstruction prototypes. There are simply far too many possible configurations to test individually with DFT.

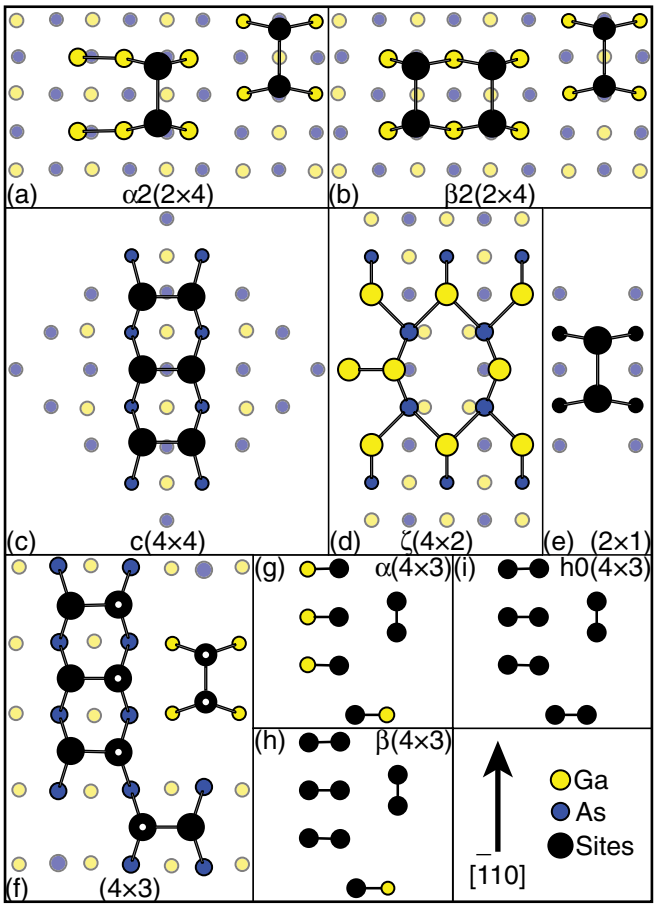

FIG. 1. (Color online) Diagram of the (a) $\alpha 2(2 \times 4)$, (b) $\beta 2(2 \times 4)$, (c) $c(4 \times 4)$, (d) $\zeta(4 \times 2)$, (e) (2×1), and (f) (4×3) surface reconstructions considered in DFT calculations. The α, β, and $h0(4 \times 3)$ variants are shown in (g)–(i). Either Ga, As, or Bi may occupy the sites in black, while black sites with white dots only allow As or Bi.

In order to rigorously investigate the energetic effects of configuration, we use the cluster expansion formalism.[30] For each reconstruction prototype, the cluster expansion predicts the surface energy of an arbitrary configuration of species on the lattice sites in terms of configuration dependent basis functions. The basis function coefficients, known as effective cluster interactions (ECIs), are fit to DFT energies calculated for a subset of configurations and describe the energetic preference for correlated occupancy of a collection of surface sites. The largest ECIs dominate the behavior of the system, enabling accurate prediction of configuration energies using only a finite set of ECIs. The most important ECIs are selected using a genetic algorithm[31] to minimize the cross validation score. Previous use of the cluster expansion method on InGaAs surfaces has demonstrated its effectiveness in determining

surface structure.[32] Four separate cluster expansions were constructed, one each for the $c(4 \times 4)$, (4×3), and (2×1) reconstruction prototypes, and one to describe the combined $\alpha 2(2 \times 4)$ and $\beta 2(2 \times 4)$ prototypes on the same lattice. Ga, As, or Bi atoms may occupy the black sites in Fig. 1, while only As or Bi may occupy the black sites with white dots in Fig. 1(f). Energies of the various configurations were calculated using density functional theory (DFT) within the local density approximation (LDA). Ultrasoft pseudopotentials were used to describe the interaction of the valence electrons with the core states of Ga, As, Bi, and the pseudo-H. All electronic structure calculations were performed with the Vienna *ab initio* simulation package (VASP).[33] Each configuration was constructed in a slab geometry, in which a 5-ML-thick GaAs slab is reconstructed on one face. The partially-filled electronic states of each As atom on the opposite face are passivated by two pseudo-H atoms ($Z = 0.75$). The top 4 ML and reconstructed surface were relaxed using a $12 \times 12 \times 1$ k-point mesh and a 203-eV plane-wave energy cutoff. Energies were calculated for configurations of supercells of each reconstruction primitive cell in order to parametrize long-range interactions that span several primitive cells. Supercells with twice the area of each reconstruction primitive cell were considered, or in the case of the (2×1) reconstruction, three times the primitive cell area. All ground-state configurations predicted by the cluster expansions were confirmed to be ground states using DFT and included in the final fits. The surface free energy related to the total energy E_{DFT} by the equation

$$\gamma = \frac{E_{\mathrm{DFT}} - N_{\mathrm{Ga}} E_{\mathrm{GaAs}} - N_{\mathrm{As}}^{XS} \mu_{\mathrm{As}} - N_{\mathrm{Bi}}^{XS} \mu_{\mathrm{Bi}}}{N_A} - \gamma_H, \tag{1}$$

where N_{Ga} is the number of Ga atoms in the calculated slab, N_A is the number of (1×1) surface unit cells in the surface supercell, N_{As}^{XS} and N_{Bi}^{XS} are the number of excess surface As and Bi atoms per (1×1) surface unit cell, and μ_{As} and μ_{Bi} are the As and Bi chemical potentials. E_{GaAs} is the DFT energy of bulk zinc-blende GaAs, and γ_H is the surface energy of the pseudohydrogen passivating layer per (1×1) surface unit cell.[34] Because the surface is a chemically open system, chemical potential, not composition, is the independent variable in the surface energy equation.

III. PHASE DIAGRAM

Minimization of γ over the range of possible structures and configurations with respect to chemical potential produces the 0 K Bi/GaAs surface phase diagram in Fig. 2(a). The chemical potentials are plotted with respect to their values in crystalline bulk reservoirs at 0 K, meaning that the system becomes energetically unfavorable with respect to bulk As at $\mu_{\mathrm{As}} = \mu_{\mathrm{As}}^{(\mathrm{bulk})}$ and with respect to bulk Bi at $\mu_{\mathrm{Bi}} = \mu_{\mathrm{Bi}}^{(\mathrm{bulk})}$. The predicted phase diagram closely follows many of the trends in surface phase stability that are observed experimentally. As expected, the Ga-terminated $\zeta(4 \times 2)$ reconstruction appears at low μ_{As} and μ_{Bi}, while at high μ_{As}, the diagram is dominated by the As rich $c(4 \times 4)$ reconstruction. The Bi rich (2×1) reconstruction, experimentally observed by depositing Bi onto a Ga rich GaAs surface,[21] appears at high μ_{Bi} and low μ_{As}. The $\alpha 2(2 \times 4)$, $\beta 2(2 \times 4)$, and (4×3) reconstructions occupy the central parts of the diagram. These predictions are consistent with the experimental RHEED phase diagram produced by Masnadi-Shirazi *et al.*, where the Bi rich (2×1) reconstruction exists at lower As_2:Ga ratios and higher temperatures.[27] In that work, the surface transforms to the (2×3) and then (1×3) diffraction patterns upon increasing the As overpressure, which correspond to a (4×3) surface with rows shifted along the $[\bar{1}10]$.

Figure 2(a) also shows the stable surface configurations of each reconstruction prototype. In naming the individual configurations, the numerical suffix indicates the number of Bi atoms in the surface unit cell. If the configuration is a supercell, it is specified by an improper fraction as the number of Bi atoms over the number of primitive cells in the configuration unit cell. For instance, the configuration shown in Fig. 2(g) has six Bi atoms occupying sites over 2 $c(4 \times 4)$ unit cells, defining this configuration as the $c(4 \times 4)$-6/2 configuration. This is not the same as the $c(4 \times 4)$-3 configuration, where Bi atoms occupy the same three sites in every unit cell. For illustrations of all stable configurations, please see the Supplemental Material.[35]

The (4×3) reconstruction prototype [Figs. 2(b)–2(e)] has 29 configurations, far more than the other prototypes combined. In some binary systems, such as AlSb, the (4×3) has three configurations: the $\alpha(4 \times 3)$ with four heterodimers [Fig. 1(g)], the $\beta(4 \times 3)$ with one cation-anion heterodimer [Fig. 1(h)], and the $h0(4 \times 3)$ that is comprised of only anion-anion dimers [Fig. 1(i)].[36] Our calculations show that these three anion-cation binary configurations describe three general classes of anion-cation (4×3) configurations on Bi/GaAs(001), possessing 4, 13, and 8 stable configurations, respectively. The remaining four are supercell configurations combining either $\alpha(4 \times 3)$ and $\beta(4 \times 3)$ or $\beta(4 \times 3)$ and $h0(4 \times 3)$ primitive cells. Starting from the most As rich $\beta(4 \times 3)$ configuration, the region of (4×3) stability expands as μ_{Bi} is increased, and Bi occupies the anion sites of the $\beta(4 \times 3)$ in the order indicated by labels in Fig. 2(b).

The $c(4 \times 4)$ reconstruction prototype possesses nine ground-state configurations [Figs. 2(f)–2(h)]. As expected, the $c(4 \times 4)\beta$ configuration consisting of As-As homodimers is stable at high μ_{As} and low μ_{Bi}. As μ_{Bi} increases, Bi occupies specific sites on the reconstruction. For high μ_{As} and μ_{Bi} all six of the dimer sites contain Bi, producing the $c(4 \times 4)$-6 configuration [Fig. 2(h)]. The $c(4 \times 4)\alpha$ configuration consists of Ga-As heterodimers as described by Ohtake,[26] but our calculations show no stable Bi-containing $c(4 \times 4)\alpha$ configurations.

The remaining reconstruction prototypes only possess one or two configurations each. The metallic (2×1)-2 configuration is the only stable (2×1) configuration and consists entirely of Bi-Bi homodimers bound to Ga atoms in the second layer. This structure does not obey the electron counting rule. By allowing second-layer sites to be occupied by Ga, As, or Bi, configurations of the (2×1) prototype can be found that do obey the electron counting rule, as proposed by Laukkanen *et al.*[20,21] to explain the existence of semiconducting (2×1) regions. However, our calculations show that there is no configuration of the (2×1) containing $\mathrm{Bi_{Ga}}$ or $\mathrm{As_{Ga}}$ antisite defects, in contrast to the experimental result. It is possible that these semiconducting regions arise from bulk phenomena that

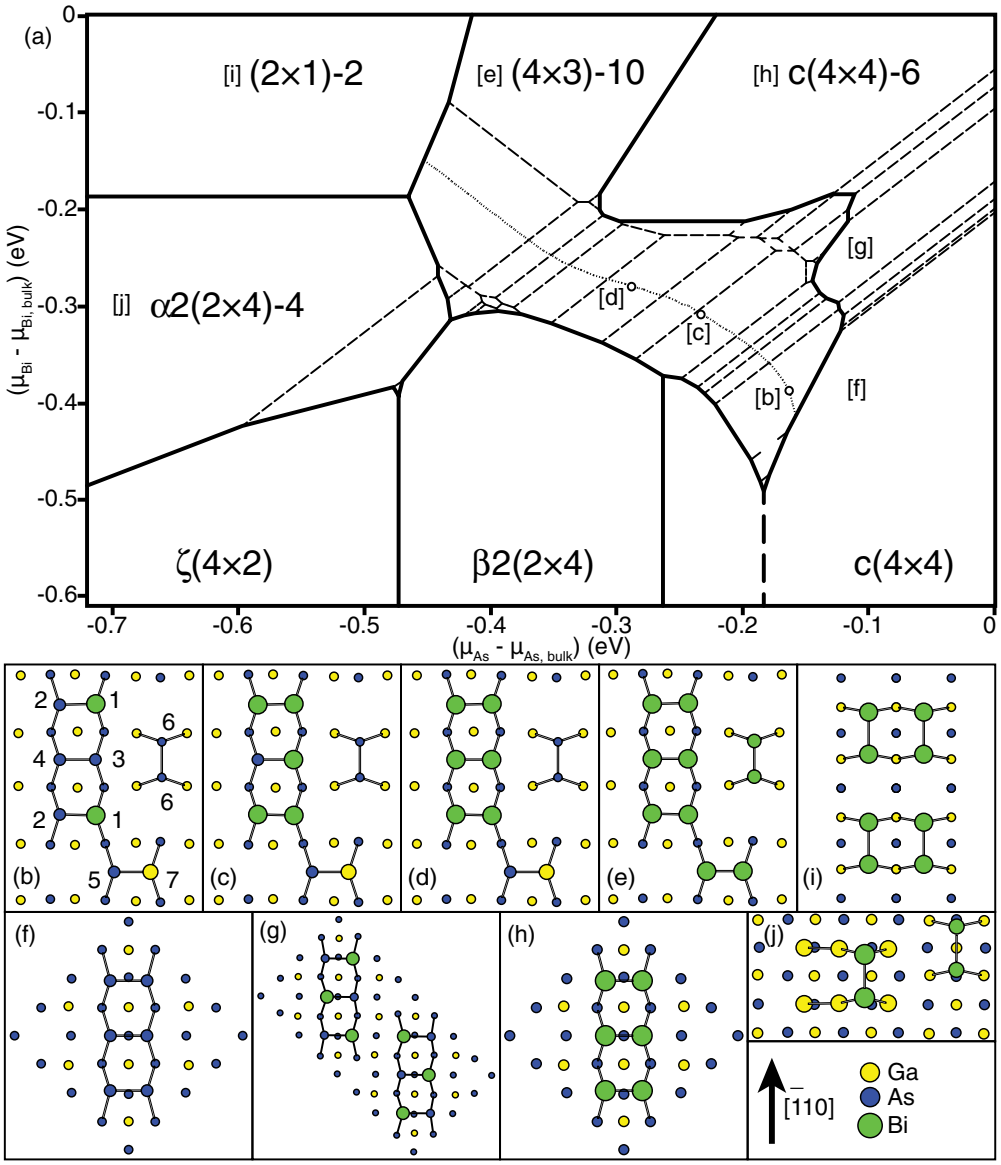

FIG. 2. (Color online) (a) Phase diagram of the Bi-terminated GaAs(001) surface reconstructions as a function of Bi and As chemical potentials. Thick solid lines separate the different reconstructions from one another, while dashed lines separate the individual configurations within each reconstruction. The thicker dotted line in the $c(4 \times 4)$ reconstruction region separates the $c(4 \times 4)\alpha$ reconstruction on the left of the line from the $c(4 \times 4)\beta$ configurations on the right. The entropy curves presented in Fig. 5 are plotted along the dotted line, with the open circles indicating where Monte Carlo cooling runs were performed. The letters in brackets correspond to the configurations of the region on the phase diagram. Stable configurations include the (b) $\beta(4 \times 3)$-2, (c) $\beta(4 \times 3)$-5, (d) $\beta(4 \times 3)$-6, (e) $h0(4 \times 3)$-10, (f) $c(4 \times 4)$, (g) $c(4 \times 4)$-6/2, (h) $c(4 \times 4)$-6, (i) (2×1)-2, and (j) $\alpha 2(2 \times 4)$-4. The order of Bi occupation in the $\beta(4 \times 3)$ reconstruction is given in (b); sites with the same number are symmetrically degenerate.

allow charge transfer to the surface rather than a consequence of the structure of the surface, achieving surface charge neutrality without antisite defects. In the $\alpha 2(2 \times 4)$ reconstruction [Fig. 1(a)], the $\alpha 2(2 \times 4)$-4 [Fig. 2(j)] and $\alpha 2(2 \times 4)$-3 (see the Supplemental Material)[35] configurations are stable. The $\beta 2(2 \times 4)$ reconstruction [Fig. 1(b)] does not accommodate Bi substitution and is only stable in the all-As configuration.

IV. MONTE CARLO SIMULATIONS

In order to quantify fluctuations in the surface composition of the Bi/GaAs(001) surface at finite temperature, grand canonical Monte Carlo simulations were performed for the (4×3) and (2×1) prototypes. The simulations were conducted along a cooling path from $530n \times C$ to $-270n \times C$ in $10n \times C$ increments at fixed (μ_{Bi}, μ_{As}) chemical potential points depicted in Fig. 2(a). At every point in (μ_{Bi}, μ_{As}, T) space, a substitution was attempted at each site of the 256-unit-cell simulation 10 000 times on average; the system was allowed to equilibrate for the first 5000 passes, after which ensemble averages were recorded for the final 5000 passes.

Monte Carlo results show that the (2×1) surface possesses strong configurational order and composition uniformity, even at synthesis temperatures, as shown in the instantaneous

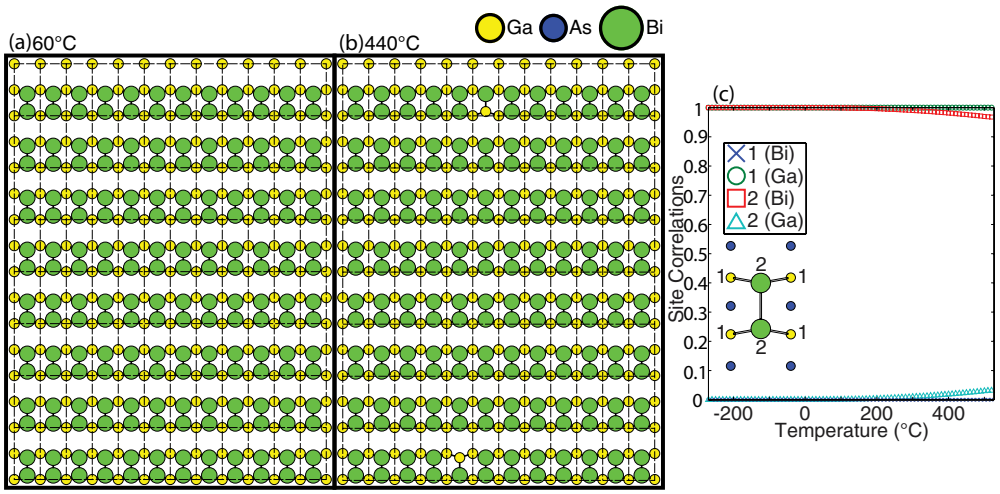

FIG. 3. (Color online) MC surface snapshots of the (2×1)-2 configuration ($\mu_{\mathrm{Bi}} = -0.1$ eV, $\mu_{\mathrm{As}} = -0.7$ eV) at (a) 60 °C and (b) 440 °C. The snapshot at −60 °C is not shown, as it is the same as part (a). The average site occupations $\langle p_i \rangle$ are plotted in (c). No As correlations were found for either site 1 or 2 and are not plotted.

simulation snapshots of the surface shown in Figs. 3(a) and 3(b). The surface exhibits occasional Bi-Ga heterodimers, visible in Fig. 3(b). Figure 3(c) shows the average site occupation of Bi in the dimer sites and Ga in the second layer sites as a function of temperature, and demonstrates the site occupation is insensitive to temperature. Over this temperature range studied here, there is no Bi occupation of the second layer sites and <5% Ga occupation of the dimer sites at typical growth temperatures.

Analysis of the (4×3) surface focused on the dominant $\beta(4 \times 3)$ variant. The (4×3) cluster expansion predicts Ga occupation of sites 1, 3, or 5 and Bi or Ga occupation of the trench dimer sites as energetically unfavorable. Trench dimer substitution was therefore neglected in the simulation, and Ga substitution was restricted to sites 2, 4, and 7. This simplification of the model enabled higher fidelity in predicting site substitution energies while still allowing the description of most thermally accessible configurations of the surface. Figure 4 shows instantaneous snapshots of the simulated surface at −60 °C, 60 °C, and 440 °C at a chemical potential corresponding to the open circle labeled [b] in Fig. 2(a), where x_{Bi}, x_{As}, and x_{Ga} varies with temperature. Qualitatively, the configurational surface order is largely maintained at −60 °C [Fig. 4(a)], where most of the unit cells match the $\beta(4 \times 3)$-2 ground state. The order degrades rapidly, with only a handful of unit cells remaining at 60 °C [Fig. 4(b)], until virtually no configurational surface order remains at a typical deposition temperature of 440 °C [Fig. 4(c)]. This corroborates the experimentally observed $(n \times 3)$ reconstruction configurational disorder seen by Duzik *et al.*[19]

A more quantitative approach of measuring configurational disorder is to compare the entropy of the surface to the entropy of an ideal surface with no correlation between species. Monte Carlo results were integrated to obtain the finite temperature surface free energy, from which the entropy can be easily obtained. The degree of configurational disorder can be measured quantitatively by the surface excess entropy s^{XS} calculated from Monte Carlo simulations. s^{XS} is obtained by first integrating to determine the finite-temperature surface free energy $\gamma(\mu_{\mathrm{As}}, \mu_{\mathrm{Bi}}, T)$, starting from a point in $(\mu_{\mathrm{As}}, \mu_{\mathrm{Bi}}, T)$ where the entropy is known (e.g., when all sites are occupied by a single species). The surface excess entropy can then be obtained using the relation $s^{XS} = (\Omega - \gamma)/T$, where Ω is the generalized surface enthalpy, defined as

$$\Omega = \left(\langle E^{XS} \rangle - \mu_{\mathrm{As}} \langle N_{\mathrm{As}}^{XS} \rangle - \mu_{\mathrm{Bi}} \langle N_{\mathrm{Bi}}^{XS} \rangle\right) / N_A. \qquad (2)$$

E^{XS} denotes the surface excess internal energy, and the terms enclosed by angle brackets indicate ensemble-average quantities obtained from the Monte Carlo simulation.

To examine the behavior of anion ordering at finite temperature, s^{XS} was calculated along the chemical potential contour that constrains the Ga composition of substitutional sites to one Ga atom per (4×3) cell which includes the set of $\beta(4 \times 3)$ configurations. The seven remaining substitutional sites can contain either As or Bi, and the fraction of these containing Bi is measure by X_{Bi} along this contour. Figure 5 shows s^{XS} plotted as a function of X_{Bi} for several temperatures. An analytical expression for the ideal configurational entropy along this contour of constrained composition was derived and is shown for reference as the dashed line in Fig. 5. Note that the ideal surface entropy does not go to zero at $X_{\mathrm{Bi}} = 0$ or 1, as the Ga composition of surface substitutional sites is still nonzero at these points. Note also the Monte Carlo entropy for the 440 °C does not equal the ideal surface entropy. This arises from the anion-cation ordering that is still prevalent even at high temperatures. the surface consists predominantly of $\beta(4 \times 3)$ unit cells, and thus the surface system does not form an ideal ternary mixture, but the Bi and As atoms do act as an ideal binary mixture at this temperature.

At −60 °C, the entropy of the $\beta(4 \times 3)$ reconstruction is well below that of the noninteracting system, with inflection points at $X_{\mathrm{Bi}} = 0.286$, 0.714, and 0.857 corresponding to the $\beta(4 \times 3)$-2, -5, and -6 ground states [Figs. 2(b)–2(d)]. Thus at −60 °C, the surface is ordered, taking on the character of the ground state, while the configurational ordering in the surface sites produces the observed deviation from the entropy of ideal mixing. At 60 °C, the inflection points are

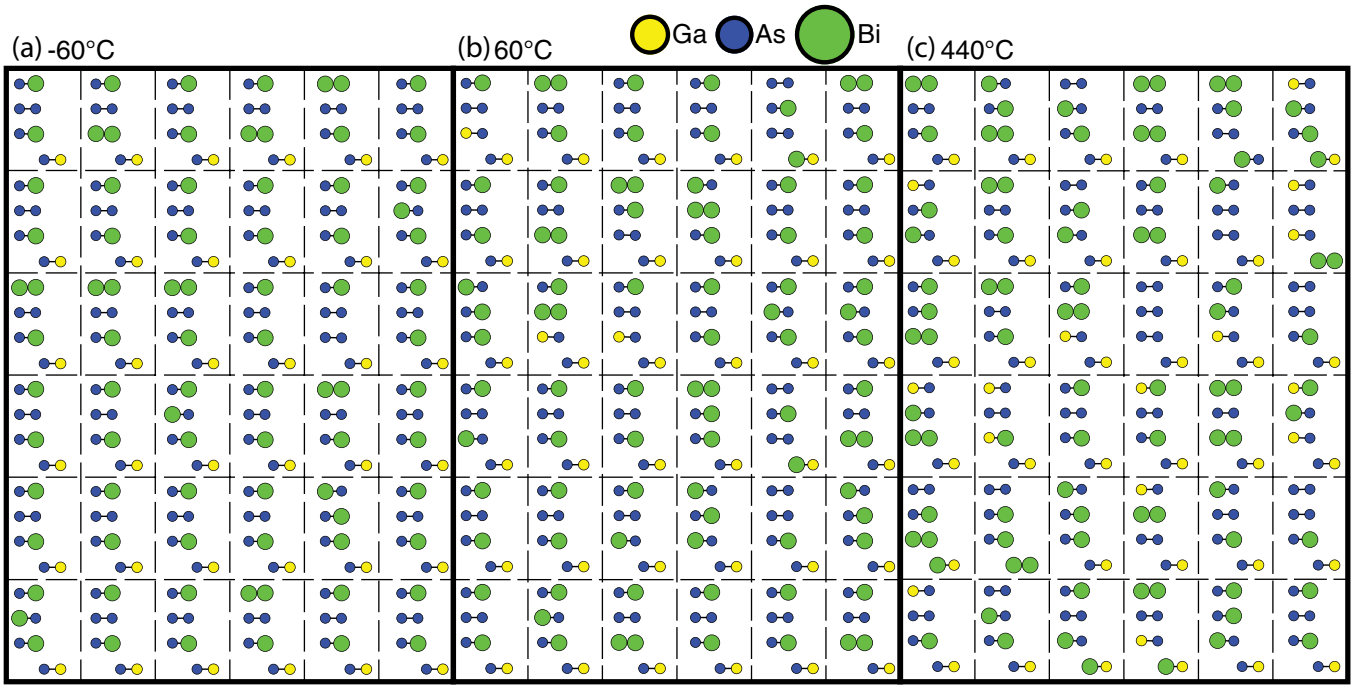

FIG. 4. (Color online) MC surface snapshots of the (4 × 3)-2 ($\mu_{Bi} = -0.80$ eV, $\mu_{As} = -1.39$ eV) at (a) −60 °C, (b) 60 °C, (c) 440 °C. Nominal composition is $x_{Bi} = 0.25$ and $x_{As} = 0.625$ at 0 K, matching the $\beta(4 \times 3)$-2 configuration. Only the top-level dimers are shown for clarity.

much less pronounced, indicating a more random filling of sites. A slight amount of ordering from the $\beta(4 \times 3)$-2 and -6 configurations still exists, but the $\beta(4 \times 3)$-5 configuration has virtually disappeared. Finally at typical experimental Bi deposition temperatures of 440 °C, the corresponding entropy approaches but is still well below that of ideal mixing. This difference occurs because the temperature is not infinite and the fact that the species distribution is not uncorrelated owing to the effective cluster interactions between sites. From this we can conclude the $\beta(4 \times 3)$ reconstruction has a strong tendency for compositional fluctuations on the anion sublattice. This interchange of Bi, As, and Ga atoms makes the surface state distribution vary from one unit cell to the next, making a well ordered experimental STM image of the (4 × 3) surface unlikely.

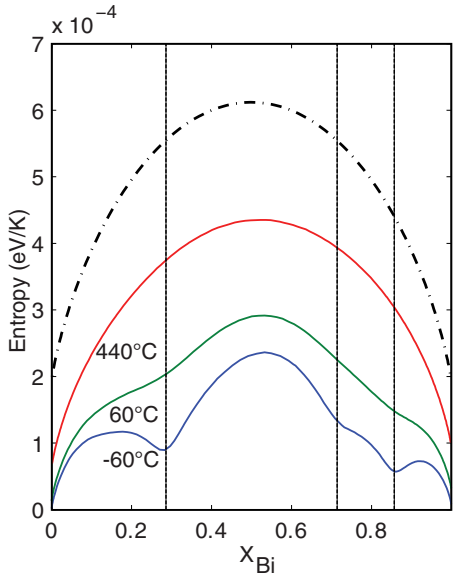

FIG. 5. (Color online) Entropy of the MC surfaces shown in Fig. 4, along the contour in chemical potential space where $x_{Bi} + x_{As} = 0.875$, or where seven of the eight dimer sites are anions. X_{Bi} refers to the fraction of the anion sites that are Bi. The dotted lines at $X_{Bi} = 0.286$, 0.714, and 0.857 correspond to $\beta(4 \times 3)$-2Bi, -5Bi, and -6Bi configurations, respectively.

To further explore the configurational ordering phenomena at the surface, we can construct site specific order parameters from Monte Carlo that measure the ordering tendencies of each symmetrically distinct site i in the unit cell. The order parameter η_i goes to 1 if site i always assumes the ground-state occupancy and goes to zero if the site occupancy is fully random, and thus proportional to the average composition. This quantity can range from 0 if sites of type i never contain species m to 1 if they always contain species m. If all sites have the same substitution energy and there are no interactions between sites, the average site occupancy $\langle p^i_{m^i} \rangle$ will be uncorrelated and will equal the average surface composition x_m. If $\langle p^i_{m^i} \rangle$ departs significantly from x_m, it reveals an ordering preference of site i for the chemical potential and temperature considered. We may define an order parameter with respect to the ground-state occupancy as

$$\eta_i = \frac{\langle p^i_{m^i} \rangle - x_{m^i}}{1 - x_{m^i}}, \tag{3}$$

where here species m^i is assumed to be the species that occupies site i in the ground-state configuration for a specific point in chemical potential space.

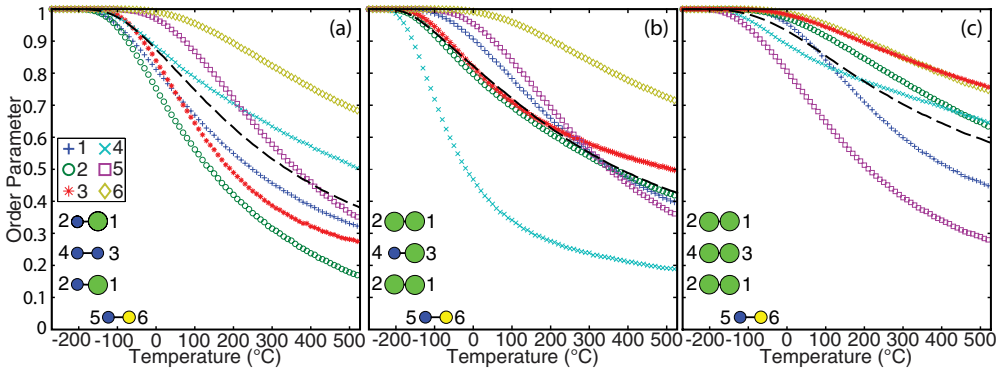

FIG. 6. (Color online) Site order parameters for the (a) $\beta(4 \times 3)$-2 ($\mu_{Bi} = -0.39$ eV, $\mu_{As} = -0.16$ eV), (b) $\beta(4 \times 3)$-5 ($\mu_{Bi} = -0.31$ eV, $\mu_{As} = -0.23$ eV), and (c) $\beta(4 \times 3)$-6 ($\mu_{Bi} = -0.28$ eV, $\mu_{As} = -0.29$ eV). Insets in each figure are models of the ground-state configurations, where Bi atoms are green, As atoms are yellow, and Ga is blue. The dashed lines represent the average of the site order parameters.

The order parameters η_i are shown in Fig. 6 for all surface sites of the (4×3), defined with respect to the $\beta(4 \times 3)$-2, -5, and -6 ground states. At temperatures near 0 K, the order parameters all approach 1, meaning that all sites assume their ground-state occupancies. With increasing temperature, η_i monotonically decreases, indicating a continuous trend toward a disordered arrangement of species across the surface sites. The order parameter of each distinct site can be compared to the average order parameter for all sites of the unit cell, which is indicated by dashed lines in Figs. 6(a)–6(c).

In all cases, site 6 is the least disordered, indicating Ga occupancy in that site is energetically very favorable. On the other hand, Fig. 6(a) shows that site 2 disorders most readily, indicating that As and Bi in the anion-anion heterodimer have a low affinity for one another. In all three cases, the system shows a preference for substitution on the As sites in the heterodimers, especially the As-Bi heterodimers. Finally, in the $\beta(4 \times 3)$-6 configuration, sites 2 and 3 have only Bi atoms as nearest neighbors, and site 1 is more volatile now since a Bi atom there can switch with the As atom in site 5. These trends in the order parameter underscore how surface diffusion can be altered by the surface reconstruction through the limiting of available sites for adatom migration. Such behavior can affect the final surface morphology and step structure on the micron length scale.

V. EXPERIMENTS

With the theoretical basis for the (4×3) reconstruction disorder in hand, we can explain the experimental observations of the surface structure that occur upon depositing Bi onto GaAs. In order to compare experiment to theory, Bi/GaAs $c(4 \times 4)$ samples were grown using molecular beam epitaxy using growth conditions described elsewhere.[19] Upon completing the buffer layer, the sample was cooled to 440 °C, then annealed for 30 minutes under a low As_4 overpressure to remove excess surface As atoms, which was completely discontinued before depositing 0.6 ML of Bi onto the GaAs $c(4 \times 4)$ surface. The resulting surface was quenched to 200 °C and transferred in vacuo into the STM chamber.

The results of the Bi deposition process are shown in Fig. 7. RHEED patterns and the surface reconstruction of the $c(4 \times 4)\alpha$ surface prior to Bi deposition are shown in Figs. 7(a)–7(c), but upon adding Bi to the surface, the RHEED and STM show a significant change in Figs. 7(d)–7(f). A (2×3) RHEED pattern has replaced the $c(4 \times 4)$ pattern, consistent with previous

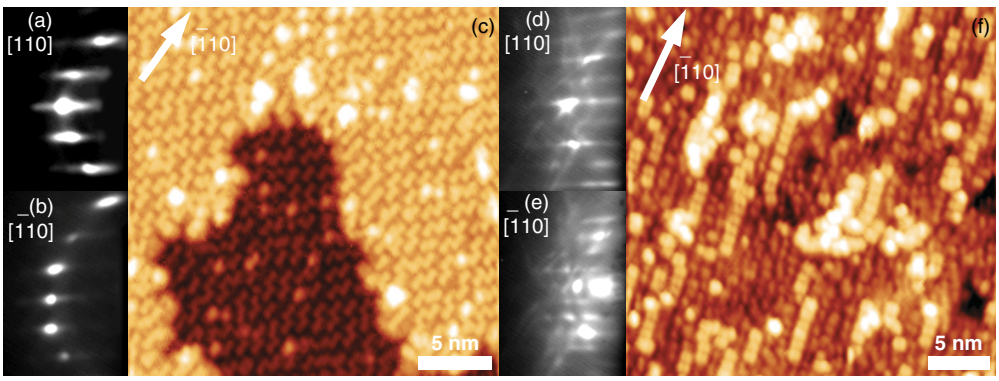

FIG. 7. (Color online) RHEED along the (a) [110] and (b) [$\bar{1}$10] zone axes and (c) filled-states STM (−2.50 V, 0.1 nA) show the typical $c(4 \times 4)\alpha$ GaAs(001)surface prior to Bi deposition. After depositing Bi, the RHEED patterns change into a (d) 2× along the [110] and a (e) 3× along the [$\bar{1}$10]. (f) Filled-states STM (−3.00 V, 0.1 nA) shows the Bi-induced surface reconstruction consists of individual segments of $\beta 2(2 \times 4)$ rows, and a disordered $(n \times 3)$ reconstruction.

work.[16,19,37] Filled states STM imaging in Fig. 7(f) shows the surface consists of a mixed reconstruction, consisting of distinct $\beta 2(2 \times 4)$ reconstruction rows separated by a $(n \times 3)$ reconstruction. Also, individual units within the rows are not uniform in appearance. This can be explained by comparing the $(n \times 3)$ reconstruction in Fig. 7(f) to the Monte Carlo surface in Fig. 4(c). Bi atoms appear most intense due to their size and greater protrusion from the surface; thus, they dominate the appearance of the $(n \times 3)$ reconstruction. Units where Bi occupies only sites 1 or 3 will appear narrower than units where sites 1–4 are also occupied. Moreover, since the kink dimer sites are not preferred for Bi occupation, most of the disorder is confined to the three chain dimers, allowing the nonuniformity in individual $(n \times 3)$ units in Fig. 7(f) while maintaining a consistent row separation.

VI. DISCUSSION

The calculated phase diagram is in excellent agreement with experimentally observed surfaces, and our predictions of the structures and configurations on the surface give important insight into the bulk configuration that results at specific growth conditions (corresponding to the chemical potentials). One of the most troublesome challenges in growing GaAsBi alloys is the incorporation of Bi. Experiments suggest that the highest incorporation of Bi can be obtained by growing on the (2×1) surface.[27] This is consistent with our results, as the (2×1)-2 has a surface concentration of Bi of unity (2 Bi/2 (1×1) area units, or $N_{\mathrm{Bi}}^{XS}/N_A = 1$), higher than even the highest Bi concentration on the (4×3) surface (10 Bi/12 (1×1) area units, or $N_{\mathrm{Bi}}^{XS}/N_A = 0.833$). The (2×1) surface reconstruction therefore enables more Bi incorporation, as more Bi is present on the growth front.

In addition to the total incorporation of Bi at surfaces, the reconstruction likely also determines the compositional uniformity. At chemical potentials that are rich in only one anion, the surface is comprised of a single structure and configuration, suggesting that compositional fluctuations are suppressed as a function of growth parameters. For instance, the Bi rich (2×1)-2 reconstruction maintains long range compositional uniformity even at high temperature according to the Monte Carlo results. Our results similarly predict the As rich $c(4 \times 4)$ surface to have uniform composition over a range of growth conditions. At chemical potentials with nearly equal numbers of both Bi and As, many configurations and structures are close in energy, leading to a high susceptibility to composition fluctuations. Indeed, the distribution of Bi and As becomes more random on the (4×3) reconstruction as a function of temperature.

GaAsBi is also known to form Bi clusters,[7] which may also be influenced by the surface reconstruction. Our results suggest that the (4×3) reconstruction can induce clustering in bulk GaAsBi. At lower Bi contents $(0.01 < x < 0.019)$, Bi pairs are observed.[7] This is consistent with the preferential occupancy of sites 1 and 2 in the $\beta(4 \times 3)$. Incoming Ga atoms can bond to the two Bi atoms and form the pairs observed in GaAsBi. Tetramers can develop in the case where there is a non-negligible probability that Bi-Bi dimers form in the next layer. Because the (4×3) surface has a high susceptibility for compositional fluctuations across the surface, this type of clustering is likely.

The details of the surface reconstruction may also influence the surface diffusivity. It is believed that adatoms diffuse along the dimer rows on the surface.[38] The (4×3) surface is comprised of different types of dimers, including As-As, Bi-Bi, As-Bi, As-Ga, and Bi-Ga, depending on growth conditions. In addition, the distribution of these dimers on the surface lattice can vary considerably. Therefore, the diffusion barrier for adatom diffusion varies as well. It is also likely that the diffusivity is reduced compared to other surfaces due to the presence of the kink dimer.

The reconstruction likely impacts where the Bi incorporates on the bulk anion sublattice as well. Norman *et al.* showed that $GaAs_{1-x}Bi_x$ possesses bulk $CuPt_B$ ordering with a Bi content of up to $x = 0.10$.[9] They attribute the $CuPt_B$ ordering to the surface atom dimerization.[39] This is consistent with our results as the (2×1)-2 reconstruction shows long range order and largely unbroken series of Bi-Bi dimers at typical growth conditions. Such a surface is necessary for appreciable bulk ordering to be detected, since different growth conditions result in a fine scale composition modulation has been attributed to the lack of the (2×1) reconstruction during growth,[9] however experimental verification of this is lacking. Nonetheless, our results suggest that other reconstructions, namely the (4×3) reconstruction, would disrupt long range compositional uniformity of the surface, making it unlikely that significant bulk ordering could be observed for films grown on these surfaces. The dimers are simply not consistent enough across the surface. Furthermore, the double anion layer termination of the (4×3) reconstruction is not conducive to bulk ordering; the anion dimers must be moved during growth and replaced with cations in order to match the bulk zinc-blende structure.

VII. CONCLUSION

Bi/GaAs(001) was investigated using experimental RHEED and STM and first principles statistical mechanical methods, establishing the phase diagram of structural and compositional stability of the (2×1), $\beta 2(2 \times 4)$, $\alpha 2(2 \times 4)$, $c(4 \times 4)$, and (4×3) reconstructions. The predictions of this phase diagram are consistent with the experimentally identified configurations both in this and previous work. Monte Carlo simulations show that the (2×1) reconstruction possesses strong compositional ordering even at typical growth temperatures, but that the distribution of Bi decorating the (4×3) approaches that of a noninteracting system. Likewise, site order parameters provide details on individual site disordering behavior with increasing temperature. Experimental observations of Bi/GaAs are consistent with the calculations, and show that depositing a submonolayer amount of Bi transforms the GaAs $c(4 \times 4)$ structures into a mixed reconstruction of $\beta 2(2 \times 4)$ rows and a compositionally disordered (4×3) row reconstruction. The details of the surface reconstructions, and the configuration of Bi atoms on the surface, have several implications for the growth of GaAsBi alloys and may explain the origins of bulk ordering and clustering observed in these systems.

ACKNOWLEDGMENTS

We gratefully acknowledge Normand Modine for his helpful insights on this work. This work was performed, in part, at the Center for Integrated Nanotechnologies, a US Department of Energy, Office of Basic Energy Sciences user facility at Los Alamos National Laboratory (Contract No. DE-AC52-06NA25396) and Sandia National Laboratories (Contract No. DE-AC04-94AL85000). The authors gratefully acknowledge the support of the National Science Foundation Materials World Network DMR 0908745. A.J.D. acknowledges funding from the National Science Foundation IGERT program DGE 0903629.

*aduzik@umich.edu
†johnct@umich.edu
‡avdv@umich.edu
§joannamm@umich.edu

[1] S. Tixier, M. Adamcyk, T. Tiedje, S. Francoeur, A. Mascarenhas, P. Wei, and F. Schiettekatte, Appl. Phys. Lett. **82**, 2245 (2003).
[2] R. N. Kini, L. Bhusal, A. J. Ptak, R. France, and A. Mascarenhas, J. Appl. Phys. **106**, 043705 (2009).
[3] K. Oe, Jpn. J. Appl. Phys. **41**, 2801 (2002).
[4] Y. Zhang, A. Mascarenhas, and L.-W. Wang, Phys. Rev. B **71**, 155201 (2005).
[5] M. J. Seong, S. Francoeur, S. Yoon, A. Mascarenhas, S. Tixier, M. Adamcyk, and T. Tiedje, Superlattices Microstruct. **37**, 394 (2005).
[6] Z. Jiang, D. A. Beaton, R. B. Lewis, A. F. Basile, T. Tiedje, and P. M. Mooney, Semicond. Sci. Technol. **26**, 055020 (2011).
[7] G. Ciatto, E. C. Young, F. Glas, J. Chen, R. A. Mori, and T. Tiedje, Phys. Rev. B **78**, 035325 (2008).
[8] D. L. Sales, E. Guerrero, J. F. Rodrigo, P. L. Galindo, A. Yanez, M. Shafi, A. Khatab, R. H. Mari, M. Henini, S. Novikov *et al.*, Appl. Phys. Lett. **98**, 101902 (2011).
[9] A. G. Norman, R. France, and A. J. Ptak, J. Vac. Sci. Technol. B **29**, 03C121 (2011).
[10] A. Stroppa, X. Duan, and M. Peressi, Mater. Sci. Eng. B **126**, 217 (2006).
[11] A. Stroppa, X. Duan, M. Peressi, D. Furlanetto, and S. Modesti, Phys. Rev. B **75**, 195335 (2007).
[12] N. Ghaderi, S. J. Hashemifar, H. Akbarzadeh, and M. Peressi, J. Appl. Phys. **102**, 074306 (2007).
[13] X. Duan, M. Peressi, and S. Baroni, Phys. Rev. B **75**, 035338 (2007).
[14] X. Duan, S. Baroni, S. Modesti, and M. Peressi, Appl. Phys. Lett. **88**, 022115 (2006).
[15] N. Ghaderi, M. Peressi, N. Binggeli, and H. Akbarzadeh, Phys. Rev. B **81**, 155311 (2010).
[16] M. Pillai, S. Kim, S. Ho, and S. Barnett, J. Vac. Sci. Technol. B **18**, 1232 (2000).
[17] E. C. Young, S. Tixier, and T. Tiedje, J. Cryst. Growth **279**, 316 (2005).
[18] S. Jun, R. Lee, C. Fetzer, J. Shurtleff, G. Stringfellow, C. Choi, and T. Seong, J. Appl. Phys. **88**, 4429 (2000).
[19] A. Duzik, J. Thomas, J. Millunchick, J. Lang *et al.*, Surf. Sci. **606**, 1203 (2012).
[20] P. Laukkanen, M. P. J. Punkkinen, H.-P. Komsa, M. Ahola-Tuomi, K. Kokko, M. Kuzmin, J. Adell, J. Sadowski, R. E. Perälä, M. Ropo *et al.*, Phys. Rev. Lett. **100**, 086101 (2008).
[21] M. P. J. Punkkinen, P. Laukkanen, H.-P. Komsa, M. Ahola-Tuomi, N. Räsänen, K. Kokko, M. Kuzmin, J. Adell, J. Sadowski, R. E. Perälä *et al.*, Phys. Rev. B **78**, 195304 (2008).
[22] M. Ahola-Tuomi, P. Laukkanen, R. E. Perälä, M. Kuzmin, J. Pakarinen, I. J. Väyrynen, and M. Adell, Surf. Sci. **600**, 2349 (2006).
[23] D. Usanmaz, M. Cakmak, and S. Ellialtioglu, J. Phys.: Condens. Matter **20**, 265003 (2008).
[24] J. C. Thomas, N. A. Modine, J. M. Millunchick, and A. Van der Ven, Phys. Rev. B **82**, 165434 (2010).
[25] M. D. Pashley, Phys. Rev. B **40**, 10481 (1989).
[26] A. Ohtake, Surf. Sci. Rep. **63**, 295 (2008).
[27] M. Masnadi-Shirazi, D. A. Beaton, R. B. Lewis, X. Lu, and T. Tiedje, J. Cryst. Growth **338**, 80 (2012).
[28] S.-H. Lee, W. Moritz, and M. Scheffler, Phys. Rev. Lett. **85**, 3890 (2000).
[29] O. Romanyuk, V. M. Kaganer, R. Shayduk, B. P. Tinkham, and W. Braun, Phys. Rev. B **77**, 235322 (2008).
[30] J. Sanchez, F. Ducastelle, and D. Gratias, Physica A **128**, 334 (1984).
[31] G. L. W. Hart, V. Blum, M. J. Walorski, and A. Zunger, Nat. Mater. **4**, 391 (2005).
[32] J. C. Thomas, J. M. Millunchick, N. A. Modine, and A. Van der Ven, Phys. Rev. B **80**, 125315 (2009).
[33] G. Kresse and J. Furthmuller, Phys. Rev. B **54**, 11169 (1996).
[34] R. R. Wixom, N. A. Modine, and G. B. Stringfellow, Phys. Rev. B **67**, 115309 (2003).
[35] See Supplemental Material at http://link.aps.org/supplemental/10.1103/PhysRevB.87.035313 for a complete labeling of all configurations in the Bi/GaAs(001) phase diagram.
[36] W. Barvosa-Carter, A. S. Bracker, J. C. Culbertson, B. Z. Nosho, B. V. Shanabrook, L. J. Whitman, H. Kim, N. A. Modine, and E. Kaxiras, Phys. Rev. Lett. **84**, 4649 (2000).
[37] E. Young, Ph.D. thesis, University of British Columbia, 2006.
[38] K. A. Fichthorn, Y. Tiwary, T. Hammerschmidt, P. Kratzer, and M. Scheffler, Phys. Rev. B **83**, 195328 (2011).
[39] S. Froyen and A. Zunger, Phys. Rev. B **53**, 4570 (1996).